ACS OMEGA

Open Access

http://pubs.acs.org/journal/acsodf

Article

High-Stability Composite Solid Polymer Electrolyte Composed of PAEPU/PP Nonwoven Fabric for Lithium-Ion Batteries

Lu Bai, Xiaoqi Chen, Fen Zhang, Haijun Zhou, Yantao Li, Peng Wang,* Na Li,* and Jijun Xiao*

Cite This: *ACS Omega* 2024, 9, 31620−31630

Read Online

ACCESS | Metrics & More | Article Recommendations | Supporting Information

ABSTRACT: Solid polymer electrolytes have attracted considerable attention, owing to their flexibility and safety. At present, poly(ethylene oxide) is the most widely studied polymer electrolyte matrix. It exhibits higher safety than the polyolefin diaphragm used in traditional lithium-ion batteries. However, it readily crystallizes at room temperature, resulting in low ionic conductivity, and the preparation process involves organic solvents. In this study, from the perspective of molecular design, solvent-free polyaspartate polyurea (PAEPU) and the cheap and easily available polypropylene (PP) nonwoven fabric were used as support materials for the PAEPU/PP composite solid polymer electrolyte (PAEPU/PP$_m$-CPE). This CPE has good thermal stability, dimensional stability, flexibility, and mechanical properties. Among the different CPEs that were analyzed, PAEPU/PP$_{10}$-CPE@20 had the highest ionic conductivity, which was reinforced with 10 g/m^2 PP nonwoven fabric and the content of lithium salt was 20 wt %. Furthermore, PAEPU/PP$_{10}$-CPE@20 exhibited the highest electrochemical stability with an electrochemical window value of 5.53 V. Moreover, the capacity retention rate of the Li//PAEPU/PP$_{10}$-CPE@20//LiFePO$_4$ half-cell was 96.82% after 150 cycles at 0.05 C and 60 °C, and the capacity recovery rate in the rate test reached 98.81%.

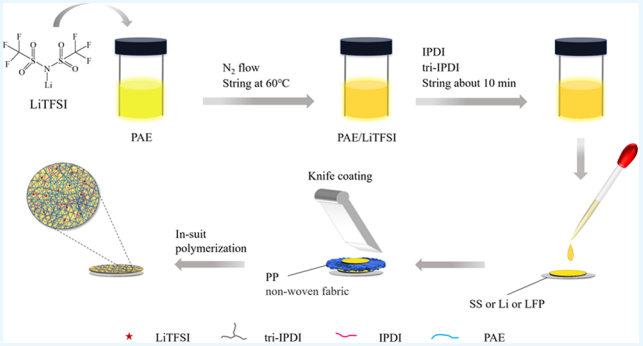

1. INTRODUCTION

The lithium-ion battery (LIB) has numerous benefits, including its high energy density, minimal self-discharge, long cycle lifespan, and absence of any memory effect, rendering it an indispensable and outstanding energy storage device.[1−4] LIBs serve as the primary power sources for electric vehicles and are important in aerospace applications. Nonetheless, the organic liquid electrolyte utilized in conventional lithium-ion batteries poses potential safety hazards, such as electrolyte volatilization, leakages, and flammability.[5−7] In addition, the lithium dendrites produced by the uneven deposition of lithium will puncture the diaphragm[8−10] and cause short circuits, leading to serious safety problems. Therefore, the use of solid electrolytes instead of traditional liquid electrolytes has been proposed.[11−14] Inorganic solid electrolytes and polymer solid electrolytes are the most popular solid electrolytes being researched at present. Inorganic solid electrolytes were once considered to be the best alternatives to organic liquid electrolytes due to their advantages of high ionic conductivity and wide working range. However, these exhibit problems such as high electrolyte thickness, poor machinability, poor extension, and shrinkage during the interface contact process, so they are no longer considered promising for the future development of flexible batteries. By contrast, polymer electrolytes have the characteristics such as lightweight, easy processing, and good compatibility with the electrode material.

Many polymer substrates have been studied as solid polymer electrolytes, such as poly(ethylene oxide) (PEO),[15−17] poly(vinylene carbonate) (PVC),[18] poly(ethylene carbonate) (PEC),[19,20] polyacrylonitrile (PAN),[21,22] poly(vinyl alcohol) (PVA),[23] poly(methyl methacrylate) (PMMA),[24−26] and poly(vinylidene fluoride) (PVDF).[27−29] However, PEO is a typical room-temperature semicrystalline polymer structure, and its crystal domain severely limits ion migration. The ionic conductivity of the solid polymer electrolyte prepared with PEO as the matrix is relatively low: only about 10^{-7} S/cm. This greatly hinders the further development of the PEO-Li salt polymer electrolyte system. Therefore, researchers have studied the above problems and proposed solutions from multiple perspectives, and the modified polymer matrix is not limited to PEO. The purpose of modification is to improve not only the ionic conductivity at room temperature but also the mechanical strength, electrochemical stability, cycle life, and electrode/electrolyte interface contact stability.

Received: February 21, 2024
Revised: April 30, 2024
Accepted: May 7, 2024
Published: July 12, 2024

Copolymerization,[30,31] cross-linking,[32−34] branching,[35,36] and other modification methods break the long-range ordered structure of the chain segment from the molecular structure, significantly reduce the glass transition temperature of the polymer electrolyte, and make the chain segment soft and suitable for easily transporting lithium ions. Other modification methods include blending,[37,38] the addition of an appropriate plasticizer,[39,40] the preparation of organic−inorganic composites,[41−45] etc. The polymer electrolyte system, in which an inorganic filler was introduced, was called a composite solid polymer electrolyte (CPE). However, in recent times, the range of composite electrolytes has become increasingly wider. In addition to the combination of the polymer electrolyte with packing or three-dimensional network structure to broaden the ion transport channel and promote ion conduction, it can also be combined with some polymer films, including nonwoven fabrics.

Wan et al.[46] prepared an ultrathin composite polymer electrolyte by filling an 8.6-μm-thick nanoporous polyimide (PI) film with PEO/LiTFSI. The results show that the arrangement of polymer chains is conducive to ion diffusion, and the existence of vertical nanochannels can improve the ionic conductivity (2.3×10^{-4} S/cm, 30 °C). The ionic conductivity can be cycled 200 times at 60 °C and C/2. Yao et al.[47] reported a modified polyethylene (PE) membrane used as the matrix, and the porous polymer interface layer poly(methyl methacrylate)-polystyrene (PMMA−PS) was attached to both sides of the ultrathin PE membrane by the phase transformation method, before being filled with poly(ethylene glycol) methyl ether acrylate and lithium salt. An ultrathin solid polymer electrolyte was prepared. The ionic conductivity of a 10-μm-thick sample of the solid polymer electrolyte was as high as 34.84 mS at room temperature, and it had excellent mechanical properties. The $LiFePO_4$//Li soft pack battery composed of this electrolyte has an initial discharge-specific capacity of 148.9 mAh/g at 1C, and a discharge-specific capacity of 113.7 mAh/g after 1000 stable cycles, with a capacity retention rate of 76.4%. Huang et al.[48] prepared a new PEO/CMC-Li@PI composite solid polymer electrolyte using PEO as the polymer matrix, modified *N*-carboxymethyl chitosan (CMC-Li) as the additive, and a PI nonwoven fabric obtained by electrostatic spinning as supporting skeleton. The outcomes of their investigation indicate that the inclusion of CMC-Li enhances the ionic conductivity of the electrolyte, while the addition of the PI nonwoven fabric improves its mechanical properties. Furthermore, when used in a $LiFePO_4$//Li solid-state battery, the PEO/CMC-Li@PI composite demonstrates commendable performance in terms of both rate capability and cycle stability, even at a high temperature of 60 °C. Consequently, the successful synthesis of the innovative PEO/CMC-Li@PI composite electrolytes presents novel avenues for the design and development of solid polymer electrolytes.

In addition, various polymer materials have been used for the design, modification, and optimization of porous membranes to prepare polymer electrolytes and deeply to explore the ion conduction mechanism, basic characteristics, and potential applications of polymer composite electrolytes in lithium-ion battery systems.[49,50]

Nonwoven fabrics have garnered significant attention due to their remarkable flexibility and affordability. In comparison to microfiber production techniques such as electrospinning, the techniques for the manufacturing of nonwoven fabrics have the advantages of a wide range of raw material sources, a simple and flexible process, and the controllability of the fiber structure. Therefore, nonwoven fabrics find applications in solid lithium metal batteries, thereby driving the progress of battery technology.[51,52] Introducing nonwoven fabrics can enhance the mechanical properties of composite polymer electrolytes, while certain types of nonwoven fabrics containing polar groups, such as polyamide nonwoven fabrics, can also facilitate the transfer of lithium ions by providing transport channels for lithium ions.

Therefore, based on previous work,[53] polyaspartate polyurea (PAEPU), a polymer with a secondary amine group and the same EO structural unit as PEO, was used to prepare PAEPU/polypropylene (PP) nonwoven composite solid polymer electrolyte (PAEPU/PP_m-CPE). It should be noted that PAEPU is obtained by the reaction of polyaspartic ester (PAE) with isophorone diisocyanate (IPDI) and isophorone diisocyanate trimer (tri-IPDI). The series of composite solid polymer electrolytes is denoted as PAEPU/PP_m-CPE@*X*, where *m* is 10 or 20, i.e., representing the weight of the PP nonwoven fabric of 10 or 20 g/m^2 (referred to as PP_{10} or PP_{20}, respectively), and *X* is 15, 20, 25, or 30, representing the lithium salt content of 15, 20, 25, or 30 wt %, respectively. By characterizing the microstructure, thermal stability, crystallinity, mechanical properties, and related electrochemical properties, the possibility for the application of the CPE in the direction of lithium secondary battery was explored. The results show that the mechanical properties of the composite solid polymer electrolyte are improved. At the same time, the composite solid polymer electrolyte has good dimensional stability and thermal stability as well as good cycling and rate performance.

2. RESULTS AND DISCUSSION

2.1. Fourier-Transform Infrared (FT-IR) Characterization. The FT-IR spectra of PAEPU/PP_{10}-CPE@*X* are shown in Figure 1. No characteristic absorption peak of the isocyanate group is visible at 2270 cm^{-1}. Furthermore, S═O and C−F absorption peaks of lithium salt LiTFSI are observed at 1058 and 1190 cm^{-1}, respectively. Moreover, the addition of the lithium salt makes the peak of the ether oxygen group (C−O−C) in the polymer chain segment shift from 1094 to 1091−

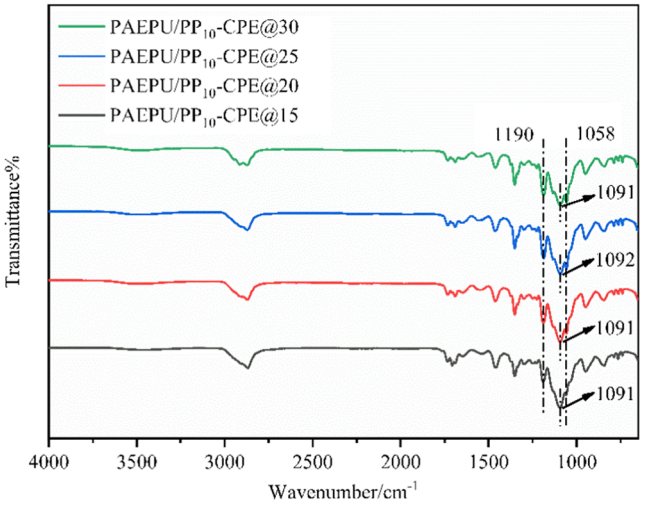

Figure 1. FT-IR spectra of PAEPU/PP_{10}-CPE@*X*.

https://doi.org/10.1021/acsomega.4c01669
ACS Omega 2024, 9, 31620−31630

Scheme 1. Interaction Between the Polymer Matrix and Li^+ in PAEPU/PP_m-CPE

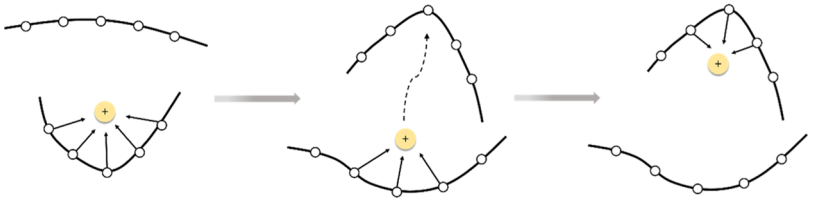

1092 cm^{-1}. This phenomenon of the C−O−C stretching band shifting toward a lower wavenumber is also observed in the PEO system,[54] which is due to the interaction between Li^+ and C−O−C. The interaction mechanism between the polymer of the composite solid polymer electrolyte and Li^+ in lithium salt is shown in Scheme 1.

2.2. Viscoelastic Behavior. Rheological test results of PAEPU/PP_{10}-CPE@*X* with a small-strain frequency conversion at 80 °C are shown in Figure 2. The stored energy modulus (G') represents the elastic property, and the loss modulus (G'') represents the viscous property. Figure 2 shows that the CPE is viscoelastic, and in the frequency range of 10^3−10^{-1} rad/s, G' is larger than G'', indicating solid properties; with the increase of the lithium content, G' shows an increased frequency correlation, showing liquid properties. This may be the result of a combination of two factors: on the one hand, the gradual increase in the lithium salt content and the increase in the number of hydrogen bonds formed between lithium ion and polymer make the CPE behave as a solid; on the other hand, when the content of lithium is too much, the "isolation" effect of lithium salt and the PP nonwoven fabric makes the reaction of −NH and −NCO insufficient, decreasing the molecular weight of the polymer, and the CPE presents liquid characteristics. In summary, liquid properties play a dominant role, so the viscosity of the composite solid polymer electrolyte increases, leading to an increase in frequency dependence.

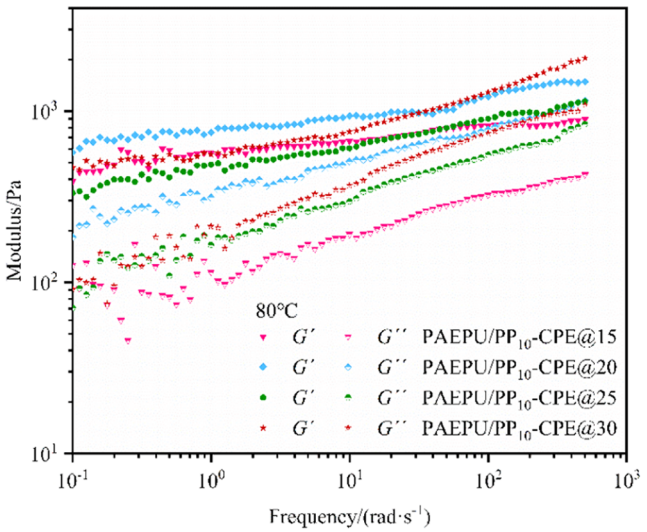

Figure 2. Modulus−frequency curve of PAEPU/PP_{10}-CPE@*X*.

2.3. Microscale Morphology and Elemental Distribution. Scanning electron microscopy (SEM) was used to observe the surface morphology of the CPE and the electrode morphology before and after the coating of the CPE, and EDS tests were conducted to characterize the distribution of the elements. The SEM and EDS results are shown in Figures 3 and 4.

As shown in Figure 3a−d, the microscale morphology of PAEPU/PP_{10}-CPE@*X* shows that the pores of the PP film are filled and no pores are visible at any lithium content. Furthermore, the gel content gradually decreases with the increase in the lithium content. Moreover, EDS was conducted on PAEPU/PP_{10}-CPE@20 as an example. As shown in Figure 3e,f, LiTFSI elements F and S are evenly distributed.

Generally, the process of assembling solid-state lithium batteries is as follows: the electrolyte is often prepared as a film and then punched by a punching machine to obtain a solid electrolyte sheet sandwiched between the cathode electrode sheet and the anode lithium sheet to assemble a button cell. The contact between the two electrodes is not sufficient, and

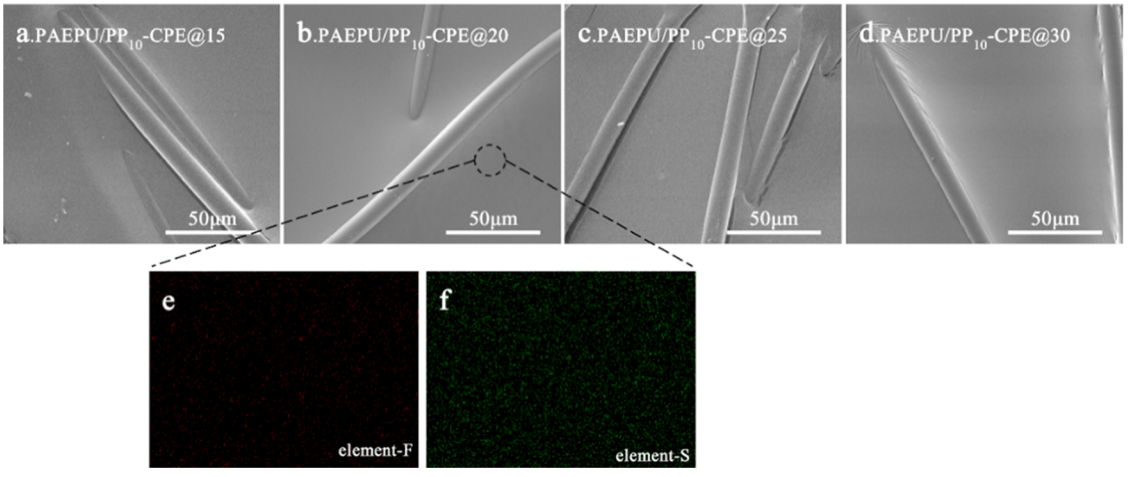

Figure 3. SEM and EDS of PAEPU/PP_{10}-CPE@*X*: (a−d) SEM image. (e, f) EDS mapping of elements F and S of PAEPU/PP_{10}-CPE@20.

https://doi.org/10.1021/acsomega.4c01669
ACS Omega 2024, 9, 31620−31630

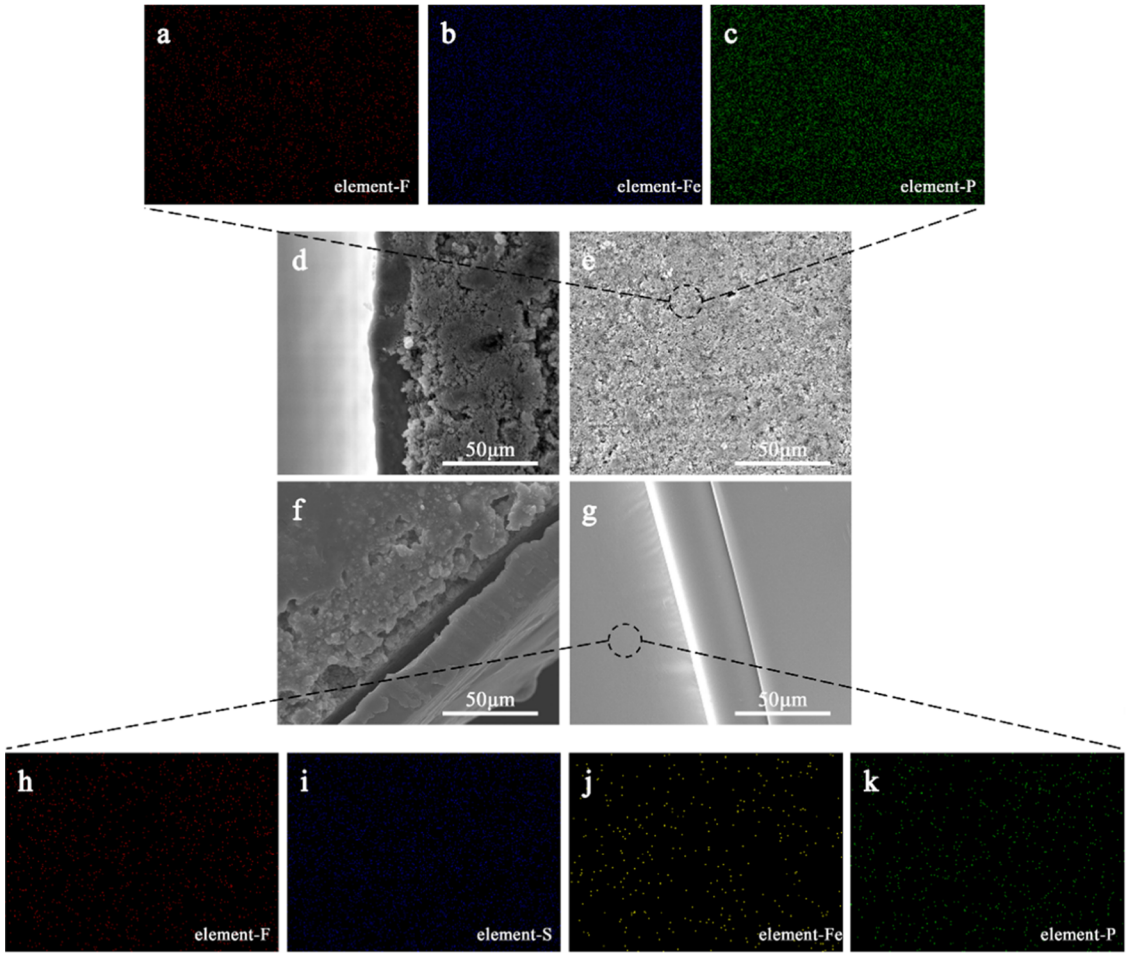

Figure 4. SEM and EDS of cathode supported CPE: (a−c) EDS mapping of elements F, Fe, and P of the cathode plate. (d) Cross-section of the cathode plate. (e) Upper surface of the cathode plate. (f) Cross-section of the cathode plate coated with PAEPU/PP_{10}-CPE@20. (g) Upper surface of the cathode plate coated with PAEPU/PP_{10}-CPE@20. (h−k) EDS mapping of F, S, Fe, and P elements of the cathode plate coated with PAEPU/PP_{10}-CPE@20.

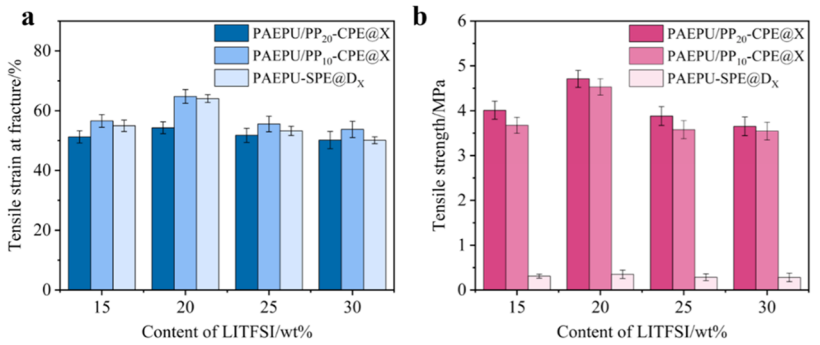

Figure 5. Mechanical properties of PAEPU/PP_m-CPE@X and PAEPU-SPE@D_X: (a) tensile strain at fracture and (b) tensile strength.

the interface compatibility is poor, resulting in a large interface impedance that causes deterioration of battery performance. In the process of preparation, the composite solid electrolyte is obtained by in situ polymerization directly on the cathode pole piece, which not only improves the contact between the electrolyte and the electrode but also fills the internal gap of the pole piece, thus resulting in a stable electrode/electrolyte interface.

Figure 4e shows the SEM image of the surface of the coated CPE pole piece: a loose and porous structure is formed between the active materials of the pole piece. Figure 4g shows the coated CPE: the surface is dense and smooth without pores. Furthermore, the SEM image of the cross-section of the pole piece in Figure 4d shows that the active materials are tightly packed on the aluminum foil, as well as the SEM image in Figure 4f. Thus, the electrolyte is in close contact with the cathode electrode, and the gap between the aluminum foil and the active material is caused by cutting with scissors during the sample preparation process.

The EDS test was carried out on the pole piece before and after CPE coating, and its structure is shown in Figure 4a−c,h−k. First, as shown in Figure 4a−c, the characteristic

https://doi.org/10.1021/acsomega.4c01669
ACS Omega 2024, 9, 31620−31630

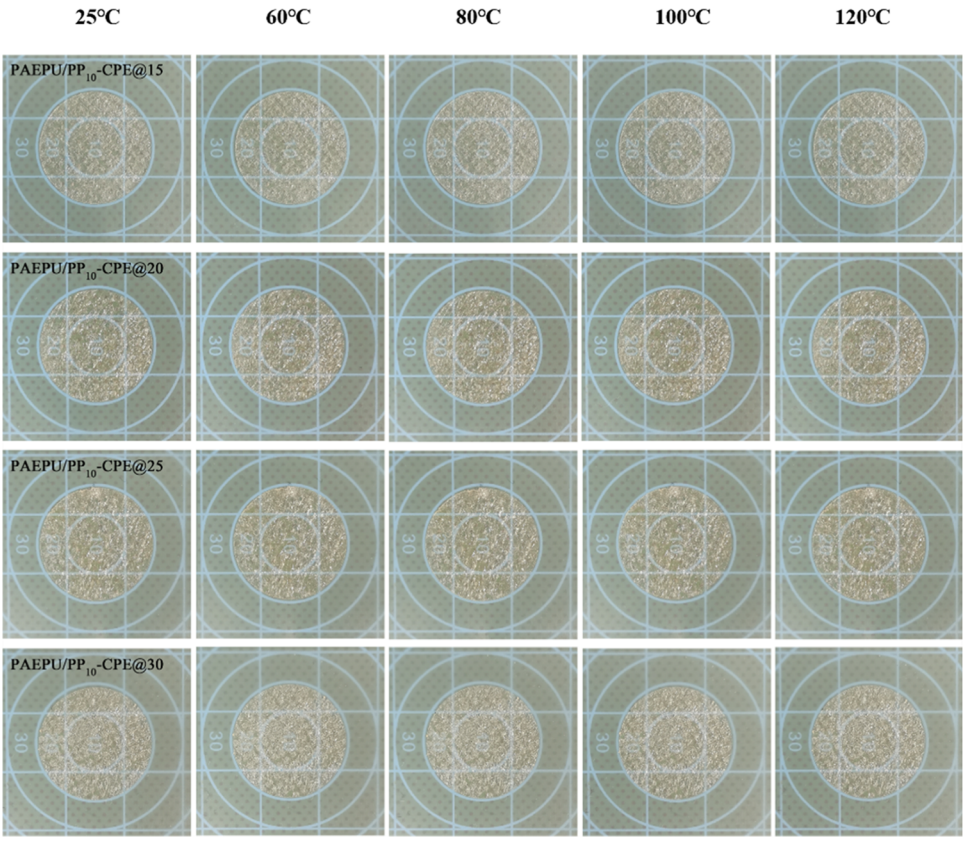

Figure 6. Schematic diagram of the dimensional stability of PAEPU/PP_{10}-CPE@*X*.

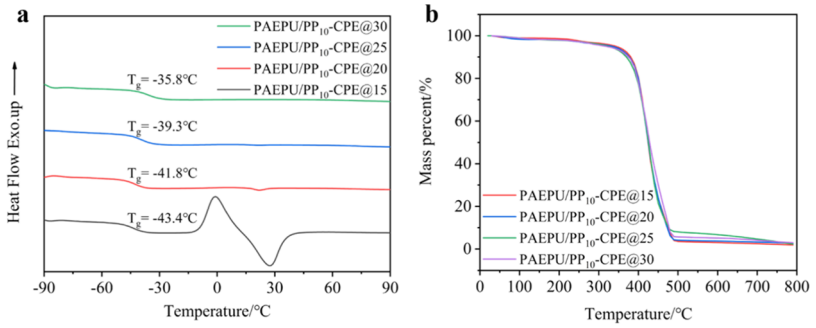

Figure 7. Curves of PAEPU/PP_{10}-CPE@*X*: (a) DSC and (b) TGA.

elements of the pole piece, i.e., Fe and P, are densely and evenly distributed. The F element originates from the binder PVDF, and it is not as dense as the Fe and P elements but is evenly distributed on the pole piece. Furthermore, after CPE coating, Fe and P elements remain uniformly distributed, but their content is greatly reduced, which shows that the CPE fully covers the surface of the pole piece.

2.4. Mechanical Properties. Good mechanical properties result in good mechanical support for the solid polymer electrolyte, thereby effectively inhibiting the growth of lithium dendrites. The PAE doped with the lithium salt of 15, 20, 25, or 30 wt % reacted with the isocynante group (IPDI/tri-IPDI molar ratio is 2:1). The obtained solid electrolyte samples were denoted as PAEPU-SPE@D_X (X = 15, 20, 25, 30). The fracture strain and tensile strength of PAEPU/PP_m-CPE@*X* and PAEPU-SPE@D_X were measured. The effects of lithium content and gram weight of the PP nonwoven fabric on the mechanical properties of the solid electrolytes were investigated. The tensile strain at break and tensile strength of the solid electrolytes are shown in Figure 5.

Figure 5 shows that with the increase in the lithium content, the fracture tensile strain and tensile strength of PAEPU/PP_m-CPE@*X* and PAEPU-SPE@D_X both increase first and then decrease. As a whole, the mechanical properties of PAEPU/PP_m-CPE@*X* are better than those of PAEPU-SPE@D_X. The mechanical tensile strength of PAEPU/PP_{20}-CPE@20 (4.71 MPa) is higher than that of PAEPU/PP_{10}-CPE@20 (4.53 MPa), while the tensile strength of PAEPU-SPE@D_{20} is only 0.35 MPa for the same lithium content. The high tensile strength of the polymer electrolyte composite with the PP nonwoven fabric is mainly attributed to the high tensile strength of the PP nonwoven fabric. The good mechanical properties impede the growth of lithium dendrites that puncture the electrolyte, resulting in contact between the positive and negative electrodes and consequent short circuits. The trend of increasing first and then decreasing may be due to

https://doi.org/10.1021/acsomega.4c01669
ACS Omega 2024, 9, 31620−31630

the added lithium salt acting as a plasticizer, which makes the nonwoven fabric and polymer electrolyte more closely, so the mechanical properties are also improved. However, when the lithium salt content is too high, some hydrogen bonds in the polymer system are broken, leading to the deterioration of the mechanical properties. The tensile strength of the solid polymer electrolyte with PP_{20} is higher than that of the solid polymer electrolyte with PP_{10}, which may be due to the denser PP nonwoven fiber filaments.

2.5. Dimensional Stability. LIBs generate heat during use, leading to an increase in the temperature. The resulting shrinkage or expansion of the electrolyte volume causes positive and negative electrodes to come into contact, resulting in a short circuit. The resultant substantial amount of heat released has a huge impact on the battery. Therefore, an ideal electrolyte should exhibit shrinkage resistance and should maintain good dimensional stability at higher temperatures.

It can be seen from Figure 6 that PAEPU/PP_{10}-CPE@*X* does not shrink at different temperatures. This phenomenon is mainly related to the improvement of mechanical properties brought about by the PP nonwoven fabric. Therefore, PAEPU/PP-CPE enhanced by the PP nonwoven fabric has good dimensional stability.

2.6. Thermal Stability. The effect of the lithium salt content on T_g of PAEPU/PP_{10}-CPE@*X* was studied by performing the DSC test. Figure 7a shows that with the increase in the LiTFSI content, T_g of the CPE gradually increases, which may be due to the complexation of lithium ions with ether oxygen groups and secondary amine groups. Strengthening, which acts as a physical cross-link, makes it difficult for the soft segment to move, resulting in an increase in T_g.

The thermal performance of the CPE was characterized by TGA, and the TGA curve of PAEPU/PP_{10}-CPE@*X* is shown in Figure 7b. Table 1 shows that with the increase in the lithium salt content, the temperature at which 5 wt % weight loss is recorded gradually decreases, but all values are above 310 °C. According to the thermal decomposition curve and data for LiTFSI in a previous report,[55] this may be explained as follows: Lithium salt readily absorbs water. Therefore, the higher the lithium salt content, the higher the water content and the higher the NCO in the system that is consumed, leading to an incomplete reaction and a reduction in the polymer molecular weight. Therefore, the higher the lithium salt content, the lower the temperature corresponding to 5 wt % weight loss.

Table 1. T_g and $T_{d,5}$ of PAEPU/PP_{10}-CPE@*X*

sample	T_g/°C	$T_{d,5}$/°C
PAEPU/PP_{10}-CPE@15	−43.4	343.77
PAEPU/PP_{10}-CPE@20	−41.8	334.80
PAEPU/PP_{10}-CPE@25	−39.3	321.47
PAEPU/PP_{10}-CPE@30	−35.8	318.79

2.7. Crystallinity. As can be seen from Figure 8, the diffraction pattern for the PP nonwoven fabric has sharp peaks at 2θ of 13.9, 16.8, 18.6, and 25.3°, indicating obvious crystallinity. The diffraction pattern of PAEPU/PP_{10}-CPE@*X* shows a wide "bulge peak" with a prominent peak. After the addition of the polyurea solid polymer electrolyte, the intensity of the sharp diffraction peaks at 2θ of 13.9, 16.8, and 18.6° reduced, and the diffraction peak at 2θ of 25.3° disappeared,

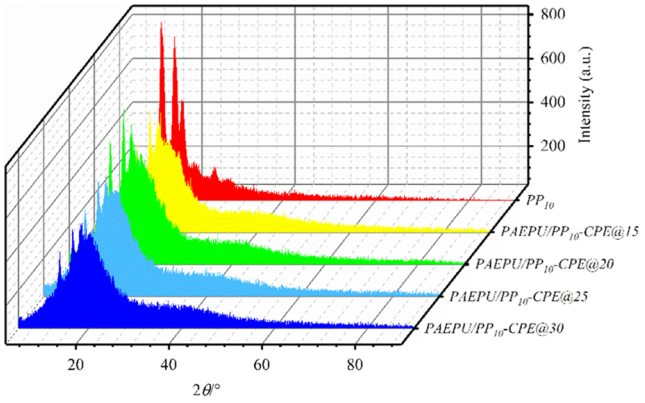

Figure 8. XRD pattern of PP_{10} and PAEPU/PP_{10}-CPE@*X*.

which may be because the filling of polyurea solid polymer electrolyte effectively covered the crystallization diffraction peaks of the PP nonwoven fabric. Combined with the DSC results, the crystal exothermic peak can be inferred to exist when the lithium contents are 15 and 20 wt %, indicating that the electrolyte is not completely amorphous. However, when the content of lithium is more than 20 wt %, the diffraction patterns indicate no crystallization.

2.8. Electrochemical Performance Characterization. The influence of the lithium content and gram weight of the PP nonwoven fabric on the ionic conductivity of the composite solid polymer electrolyte and the relationship between the temperature and conductivity were analyzed. The results are shown in Figure 9.

As can be seen from Figure 9a,c, when PAEPU/PP_{10}-CPE@*X* and PAEPU/PP_{20}-CPE@*X* are at 30 °C, the ionic conductivity increases first and then decreases with an increase in the LiTFSI content. The ionic conductivity of the two electrolytes is the highest when the lithium content is 20 wt %. The conductivity of PAEPU/PP_{10}-CPE@20 is the highest when the content of lithium is 20 wt %. The ionic conductivity of PAEPU/PP_{10}-CPE@20 is 2.46×10^{-5} S/cm at 30 °C, 1.26×10^{-4} S/cm at 60 °C, and 2.75×10^{-4} S/cm at 80 °C. The ionic conductivity of PAEPU/PP_{20}-CPE@20 is 1.62×10^{-5} S/cm at 30 °C, 8.7×10^{-5} S/cm at 60 °C, and 2.0×10^{-4} S/cm at 80 °C. However, the ionic conductivity of PAEPU/PP_{10}-CPE@*X* and PAEPU/PP_{20}-CPE@*X* increases first and then decreases at 30 °C, which may be because of two reasons: the first reason is that the number of free Li^+ carriers increases with the increase in the lithium salt concentration in the low-concentration range, resulting in a gradual increase in the conductivity, but as the concentration continues to increase, the formation of ion clusters diminishes the number of effective Li^+ carriers. The second reason is that with the increase in the lithium salt concentration, Li^+ dissociated from the lithium salt in the "complexation-decomplexation" process can not only interact with −COC− in the polymer chain segment but also complexed with a trace of −NH (which can act as a Lewis base). Whether it is the resulting lithium ion and the ether oxygen of the polymer chain segment or the competition relationship with the N coordination, it will lead to more free lithium ions, promote lithium ion transfer, and improve ionic conductivity. However, when the concentration of the lithium salt is too high, the number of carriers increases until it reaches saturation, and too many lithium ions form a large number of ion clusters. Therefore, the hydrogen bond system inside the solid polymer electrolyte is destroyed, which

https://doi.org/10.1021/acsomega.4c01669
ACS Omega 2024, 9, 31620−31630

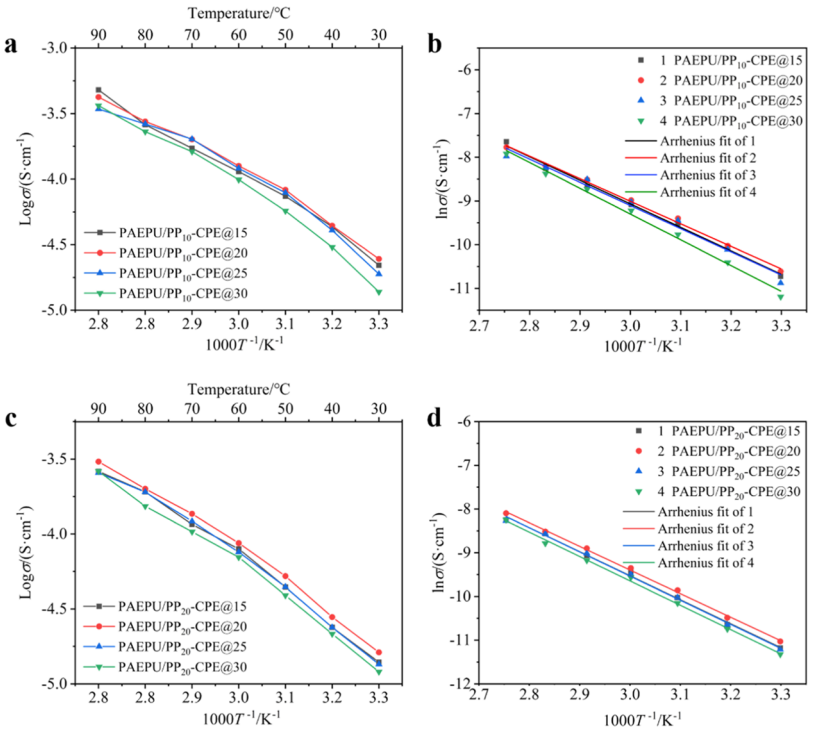

Figure 9. Temperature dependence of ionic conductivity of PAEPU/PP$_m$-CPE@*X*. (a) Ionic conductivity curve of PAEPU/PP$_{10}$-CPE@*X*. (b) Arrhenius fitting curve of PAEPU/PP$_{10}$-CPE@*X*, T = 303.15 K. (c) Ionic conductivity curve of PAEPU/PP$_{20}$-CPE@*X*. (d) Arrhenius fitting curve for PAEPU/PP$_{20}$-CPE@*X*, T = 303.15 K.

impedes the movement of polymer chain segments, thereby hindering ion conduction and leading to a reduction in conductivity.

The mechanism of the long-term transport of lithium ions in a polymer matrix can be effectively described by the Arrhenius equation. The equation that represents the relationship between the temperature and conductivity is as follows

$$\sigma(T) = A \exp\left(-\frac{E_a}{KT}\right)$$

where A represents the prefactor, E_a represents the activation energy, K represents the Boltzmann constant, and T represents the thermodynamic temperature.

Figure 9b,d shows the curve after fitting the experimental test points through the Arrhenius equation. Table S1 shows that the relationship between the ionic conductivity and temperature of the PAEPU/PP$_m$-CPE@*X* conforms to the Arrhenius equation. As the test temperature increases, the ionic conductivity increases gradually. This may be because when the temperature rises, the movement of the chain segments becomes easier and the number of effective carriers increases; therefore, the ionic conductivity gradually increases. The results of linear fitting of each sample show that the activation energy of the composite solid polymer electrolyte is low when the lithium salt content is 20 wt %, and the activation energy of PAPEPU/PP$_{10}$-CPE@20 (0.445 eV) is lower than that of PAPEPU/PP$_{20}$-CPE@20 (0.466 eV).

The results of mechanical properties and ionic conductivity of the solid polymer electrolyte samples with the PP nonwoven fabrics show that although the tensile strength of the polymer electrolyte with PP$_{20}$ is slightly higher than that of the electrolyte with PP$_{10}$, the ionic conductivity of the latter is higher than that of the former. Hence, the CPE reinforced with PP$_{10}$ is considered for other electrochemical tests.

A series of PAEPU/PP$_{10}$-CPE@*X* samples were subjected to linear voltammetry tests. As can be seen from Figure 10 and

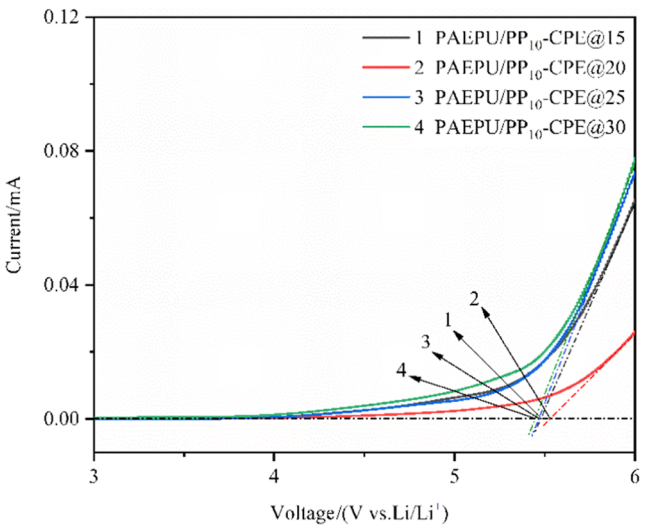

Figure 10. Linear voltammetry test curve of PAEPU/PP$_{10}$-CPE@*X*.

Table 2, the electrochemical stability window values of PAEPU/PP$_{10}$-CPE@*X* are all above 5.4 V. With an increase in the lithium salt content, the electrochemical stability window values first increase and then decrease. When the lithium salt content is 20 wt %, PAEPU/PP$_{10}$-CPE@20 shows the best electrochemical stability with an electrochemical window value of 5.53 V. In addition, when the lithium content is 15 wt %, the electrochemical stability window of PAEPU/

https://doi.org/10.1021/acsomega.4c01669
ACS Omega 2024, 9, 31620−31630

Table 2. Electrochemical Stability Window Values of PAEPU/PP_{10}-CPE@*X*

sample	value/V
PAEPU/PP_{10}-CPE@15	5.48
PAEPU/PP_{10}-CPE@20	5.53
PAEPU/PP_{10}-CPE@25	5.47
PAEPU/PP_{10}-CPE@30	5.45

PP_{10}-CPE@15 (5.48 V) is higher than that of the electrolyte system without the nonwoven fabric (5.18 V for PAEPU-SPE@D_{15}) shown in Figure S1. This may be because the high mechanical strength of the composite solid polymer electrolyte reinforced with the PP nonwoven fabric can inhibit the growth of lithium dendrites, making the interface between the electrolyte and electrode more stable, thus satisfying the requirements for high-performance lithium battery applications.

An important aspect of evaluating the battery performance is the stability of the interface between the electrode and electrolyte. In particular, the formation of a stable solid electrolyte interface (SEI) between the electrolyte and electrode enables the battery to undergo continuous and stable cycles over an extended period.

To study the stability of the interface between the electrolyte and the lithium metal electrode, the interfacial impedance of PAEPU/PP_{10}-CPE@*X* was monitored at ambient temperature, and the change in the impedance value with time was studied. As shown in Figure 11, with an increase in time, the interface impedance increases slowly until it becomes stable, indicating that a relatively stable SEI film has been formed.

To characterize the effect of the electrolyte prepared by the in situ polymerization method on the electrode/electrolyte interface, the PAEPU/PP_{10}-CPE@20 sample was used to prepare a Li//LFP battery by in situ polymerization and non-in-situ polymerization, respectively, and the AC impedance spectrum test was performed. As can be seen from Figure 12,

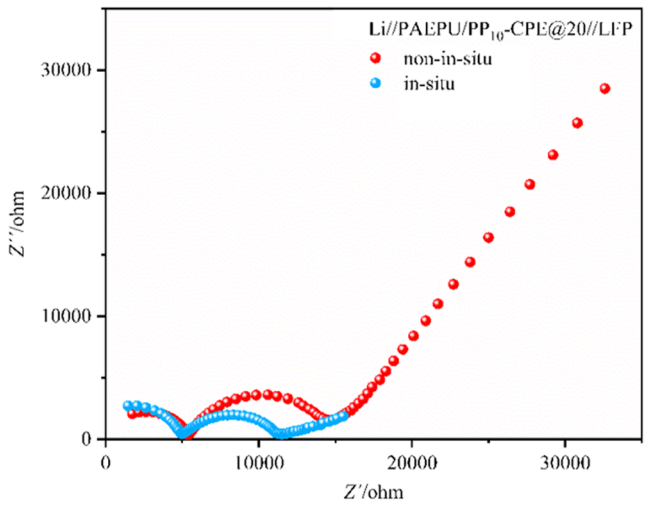

Figure 12. Nyquist comparison between in situ polymerization and non-in-situ polymerization of Li//PAEPU/PP_{10}-CPE@20//$LiFePO_4$ half battery.

the impedance value of the electrolyte prepared by in situ polymerization is 6441 Ω, much lower than that of the electrolyte obtained by non-in-situ polymerization (9292 Ω), which further confirms that the composite solid polymer electrolyte formed by in situ polymerization is effective in improving the interface stability.

Cycle and rate performances are important performance indexes of lithium batteries. The tests shown in Figure 13 were all obtained by assembling cathode-supported composite solid polymer electrolytes using the method described in Supporting Information.

Figure 13a shows the cyclic test results for the Li//PAEPU/PP_{10}-CPE@20//$LiFePO_4$ half-cell at a current density of 0.05C. For the first charge−discharge cycle, the specific discharge capacity is 141.6 mAh/g, and after 150 cycles, the

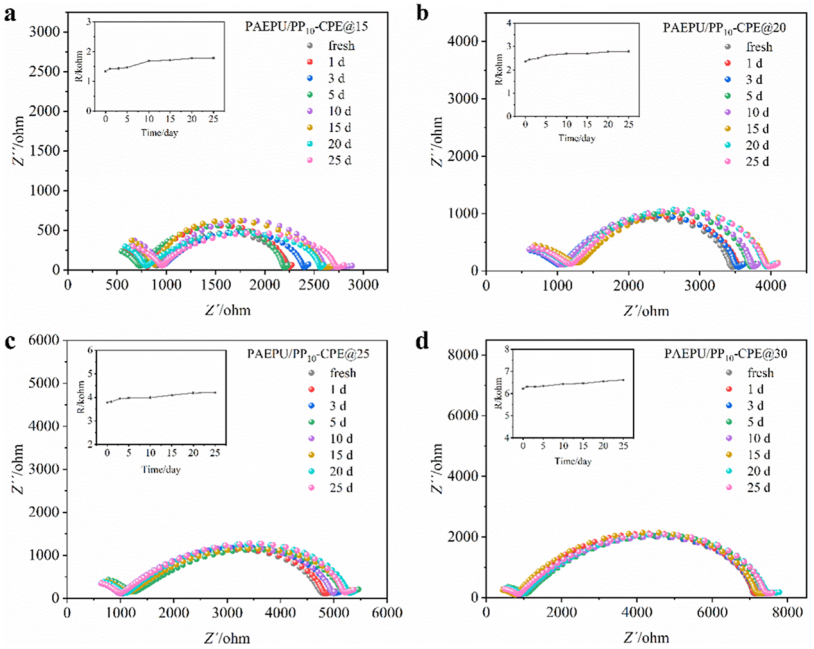

Figure 11. Nyquist plot and dot plot of PAEPU/PP_{10}-CPE@*X* interface impedance versus time. (a) PAEPU/PP_{10}-CPE@15. (b) PAEPU/PP_{10}-CPE@20. (c) PAEPU/PP_{10}-CPE@25. (d) PAEPU/PP_{10}-CPE@30.

https://doi.org/10.1021/acsomega.4c01669
ACS Omega 2024, 9, 31620−31630

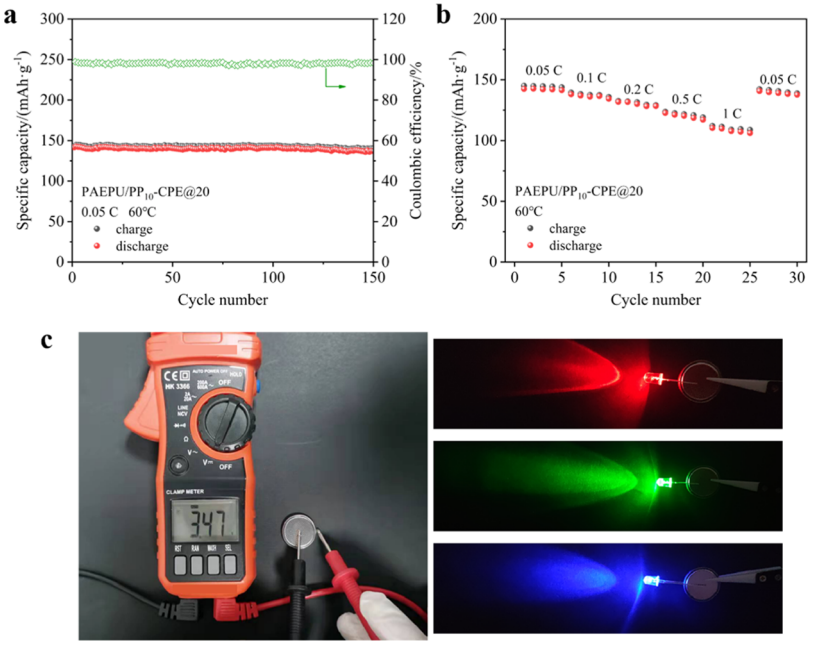

Figure 13. Electrochemical performance of Li//PAEPU/PP_{10}-CPE@20//$LiFePO_4$ half-cell. (a) Cycling performance at 0.05 and 60 °C. (b) Charge and discharge curves at 60 °C. (c) DC voltage measured using a multimeter, and the assembled half-cell could light up red, green, and blue LED lamps at room temperature.

specific discharge capacity is 137.1 mAh/g, the Coulombic efficiency is always maintained at >97% in 150 cycles, and the capacity retention rate is up to 96.82%, which shows good charge−discharge capacity reversibility. Figure 13b shows the results of the rate test for Li//PAEPU/PP_{10}-CPE@20//$LiFePO_4$ half-cell at the current density of 0.05, 0.1, 0.2, 0.5, and 1C, and the corresponding discharge-specific capacity is 142.5, 138.1, 131.8, 122.7, and 110.4 mAh/g, respectively. When the current density is from 1 to 0.05C, the discharge-specific capacity is 140.8 mAh/g, which is 98.81% of the discharge-specific capacity at the initial current density of 0.05C, and the battery capacity has little difference, showing a high capacity recovery rate, the PP nonwoven fabric reinforced composite solid polymer electrolyte has excellent rate performance. To further determine the applicability of the battery, as shown in Figure 13c, the CPE is used to assemble a Li//PAEPU/PP_{10}-CPE@20//$LiFePO_4$ button cell. The DC voltage measured by a multimeter was 3.47 V, and the red LED lamp (1.9 V), green LED lamp (2.6 V), and blue LED lamp (2.8 V) were successfully lit.

3. CONCLUSIONS

A series of composite solid polymer electrolytes were successfully prepared by combining the IPDI/tri-IPDI molar ratio of 2:1 polyurea-based all-solid polymer electrolytes with the PP nonwoven fabric of different grams. The electrolyte has good dimensional stability, thermal stability, and mechanical properties. The tensile strength of the enhanced PAEPU/PP_m-CPE@X is obviously better than that of the PAEPU-SPE@D_X. The good mechanical properties can effectively inhibit the growth of lithium dendrites, thereby minimizing the possibility of short circuits because of the direct contact between the anode and cathode resulting from the lithium dendrites puncturing the electrolyte. PAEPU/PP_{10}-CPE@20 has the highest ionic conductivity, which is 2.46×10^{-5} S/cm at 30 °C, and the electrochemical window value is 5.53 V. The Li//PAEPU/PP_{10}-CPE@20//$LiFePO_4$ half-cell exhibits a primary discharge-specific capacity of 141.6 mAh/g, and after 150 cycles, the coulomb efficiency is always maintained at above 97% with a capacity retention rate of 96.82%. When the current density is 0.05, 0.1, 0.2, 0.5, and 1C, the capacity recovery rate is 98.81%, indicating good magnification performance. Furthermore, red, green, and blue LED lights could be successfully lit, confirming good application prospects. The composite solid polymer electrolyte has the advantages of a simple preparation process, good mechanical properties, and adaption to size changes and is therefore promising for improving the safety of batteries. Therefore, this work lays the foundation for the development of wearable electronic devices and batteries with high energy density.

4. EXPERIMENTAL SECTION

The materials used in this study, the process for the preparation of the composite electrolytes, and the characterization are detailed in the Supporting Information.

■ ASSOCIATED CONTENT

Supporting Information

The Supporting Information is available free of charge at https://pubs.acs.org/doi/10.1021/acsomega.4c01669.

Materials; preparation of PAEPU/PP-CPE; electrochemical stability window of PAEPU-SPE@D_{15} at room temperature; activation energy of PAEPU/PP_{10}-CPE@X and PAEPU/PP_{20}-CPE@X (PDF)

■ AUTHOR INFORMATION

Corresponding Authors

Peng Wang − *Hebei Key Laboratory of Flexible Functional Materials, School of Materials Science and Engineering, Hebei University of Science and Technology, Shijiazhuang 050000, China;* orcid.org/0000-0001-9669-9343;
Email: wp390061130@126.com

https://doi.org/10.1021/acsomega.4c01669
ACS Omega 2024, 9, 31620−31630

Na Li − *Hebei Key Laboratory of Flexible Functional Materials, School of Materials Science and Engineering, Hebei University of Science and Technology, Shijiazhuang 050000, China*; Email: linahuaxue@163.com

Jijun Xiao − *Hebei Key Laboratory of Flexible Functional Materials, School of Materials Science and Engineering, Hebei University of Science and Technology, Shijiazhuang 050000, China*; Email: xiaojj@hebust.edu.cn

Authors

Lu Bai − *Institute of Energy Resources, Hebei Academy of Sciences, Shijiazhuang 050081, China*

Xiaoqi Chen − *Institute of Energy Resources, Hebei Academy of Sciences, Shijiazhuang 050081, China*

Fen Zhang − *Institute of Energy Resources, Hebei Academy of Sciences, Shijiazhuang 050081, China*

Haijun Zhou − *Institute of Energy Resources, Hebei Academy of Sciences, Shijiazhuang 050081, China*

Yantao Li − *Institute of Energy Resources, Hebei Academy of Sciences, Shijiazhuang 050081, China*

Complete contact information is available at: https://pubs.acs.org/10.1021/acsomega.4c01669

Notes

The authors declare no competing financial interest.

■ ACKNOWLEDGMENTS

The authors thank the financial support from the Fundamental Research Funds Pilot Project of the Hebei Academy of Sciences (2023PF03-1,2024PF01), Xingtai Key Research and Development Plan Project (2023ZZ041), and the Natural Science Foundation of Hebei Province (H2021302001).

■ REFERENCES

(1) Zhou, L.; Zhang, K.; Hu, Z.; Tao, Z.; Mai, L.; Kang, Y. M.; Chou, S. L.; Chen, J. Recent Developments on and Prospects for Electrode Materials with Hierarchical Structures for lithium-Ion Batteries. *Adv. Energy Mater.* **2018**, *8* (6), No. 1701415.

(2) Jiang, Y.; Yan, X.; Ma, Z.; Mei, P.; Xiao, W.; You, Q.; Zhang, Y. Development of the PEO Based Solid Polymer Electrolytes for All-Solid-State Lithium Ion Batteries. *Polymers* **2018**, *10* (11), 1237.

(3) Shi, K.; Xu, Z.; Huang, M.; Zou, L.; Zheng, D.; Yang, Z.; Zhang, W. Solid-State Polymer Electrolytes with Polypropylene Separator-Reinforced Sandwich Structure for Room-Temperature Lithium Ion Batteries. *J. Membr. Sci.* **2021**, *638*, No. 119713.

(4) Xia, S.; Wu, X.; Zhang, Z.; Cui, Y.; Liu, W. Practical Challenges and Future Perspectives of All-Solid-State Lithium-Metal Batteries. *Chem* **2019**, *5* (4), 753−785.

(5) Cong, L.; Liu, J.; Armand, M.; Mauger, A.; Julien, C. M.; Xie, H.; Sun, L. Role of Perfluoropolyether-Based Electrolytes in Lithium Metal Batteries: Implication for Suppressed Al Current Collector Corrosion and the Stability of Li Metal/Electrolytes Interfaces. *J. Power Sources* **2018**, *380*, 115−125.

(6) Wu, M.; Ju, Y. K.; Chae, O. B.; Jung, W. B.; Jung, H. T.; et al. Nanoscale Wrinkled Cu as a Current Collector for High-Loading Graphite Anode in Solid-State Lithium Batteries. *ACS Appl. Mater. Interfaces* **2021**, *13* (2), 2576−2583.

(7) Deng, K.; Han, D.; Ren, S.; Wang, S.; Xiao, M.; Meng, Y. Single-Ion Conducting Artificial Solid Electrolyte Interphase Layers for Dendrite-Free and Highly Stable Lithium Metal Anodes. *J. Mater. Chem. A* **2019**, *7* (21), 13113−13119.

(8) He, Y.; Qiao, Y.; Chang, Z.; Zhou, H. The Potential of Electrolyte Filled MOF Membranes as Ionic Sieves in Rechargeable Batteries. *Energy Environ. Sci.* **2019**, *12* (8), 2327−2344.

(9) Wang, T.; Salvatierra, R. V.; Tour, J. M. Detecting Li Dendrites in a Two-Electrode Battery System. *Adv. Mater.* **2019**, *31* (14), No. 1807405.

(10) Liu, Y.; Liu, Q.; Xin, L.; Liu, Y.; Yang, F.; Stach, E. A.; Xie, J. Making Li-Metal Electrodes Rechargeable by Controlling the Dendrite Growth Direction. *Nat. Energy* **2017**, *2* (7), 17083 DOI: 10.1038/nenergy.2017.83.

(11) Tarascon, J.-M.; Armand, M. Issues and Challenges Facing Rechargeable Lithium Batteries. *Nature* **2001**, *414* (6861), 359−367.

(12) Goodenough, J. B.; Park, K.-S. The Li-Ion Rechargeable Battery: A Perspective. *J. Am. Chem. Soc.* **2013**, *135* (4), 1167−1176.

(13) Cohen, S. M. The Postsynthetic Renaissance in Porous Solids. *J. Am. Chem. Soc.* **2017**, *139* (8), 2855−2863.

(14) Cheng, X.-B.; Zhang, R.; Zhao, C.-Z.; Zhang, Q. Toward Safe Lithium Metal Anode in Rechargeable Batteries: A Review. *Chem. Rev.* **2017**, *117* (15), 10403−10473.

(15) Deng, F.; Wang, X.; He, D.; Hu, J.; Gong, C.; Ye, Y. S.; Xie, X.; Xue, Z. Microporous Polymer Electrolyte Based on PVDF/PEO Star Polymer Blends for Lithium Ion Batteries. *J. Membr. Sci.* **2015**, *491*, 82−89.

(16) Mustafa, M. S.; Ghareeb, H. O.; Aziz, S. B.; Brza, M.; Al-Zangana, S.; Hadi, J. M.; Kadir, M. Electrochemical Characteristics of Glycerolized PEO-Based Polymer Electrolytes. *Membranes* **2020**, *10* (6), 116.

(17) Wen, J.; Zhao, Q.; Jiang, X.; Ji, G.; Wang, R.; Lu, G.; Long, J.; Hu, N.; Xu, C. Graphene Oxide Enabled Flexible PEO-Based Solid Polymer Electrolyte for All-Solid-State Lithium Metal Battery. *ACS Appl. Energy Mater.* **2021**, *4* (4), 3660−3669.

(18) Chai, J.; Liu, Z.; Ma, J.; Wang, J.; Liu, X.; Liu, H.; Zhang, J.; Cui, G.; Chen, L. In Situ Generation of Poly(vinylene carbonate) Based Solid Electrolyte with Interfacial Stability for $LiCoO_2$ Lithium Batteries. *Adv. Sci.* **2017**, *4* (2), No. 1600377.

(19) Kimura, K.; Hassoun, J.; Panero, S.; Scrosati, B.; Tominaga, Y. Electrochemical Properties of a Poly(ethylene carbonate)-LiTFSI Electrolyte Containing a Pyrrolidinium-Based Ionic Liquid. *Ionics* **2015**, *21*, 895−900.

(20) Kimura, K.; Yajima, M.; Tominaga, Y. A Highly-Concentrated Poly(ethylene carbonate)-Based Electrolyte for All-Solid-State Li Battery Working at Room Temperature. *Electrochem. Commun.* **2016**, *66*, 46−48.

(21) Jia, W.; Li, Z.; Wu, Z.; Wang, L.; Wu, B.; Wang, Y.; Cao, Y.; Li, J. Graphene Oxide as a Filler to Improve the Performance of PAN-$LiClO_4$ Flexible Solid Polymer Electrolyte. *Solid State Ionics* **2018**, *315*, 7−13.

(22) Hu, C.; Shen, Y.; Shen, M.; Liu, X.; Chen, H.; Liu, C.; Kang, T.; Jin, F.; Li, L.; Li, J.; et al. Superionic Conductors via Bulk Interfacial Conduction. *J. Am. Chem. Soc.* **2020**, *142* (42), 18035−18041.

(23) Varishetty, M. M.; Qiu, W.; Gao, Y.; Chen, W. Structure, Electrical and Optical Properties of ($PVA/LiAsF_6$) Polymer Composite Electrolyte Films. *Polym. Eng. Sci.* **2010**, *50* (5), 878−884.

(24) Choudhary, S. Effects of Amorphous Silica Nanoparticles and Polymer Blend Compositions on the Structural, Thermal and Dielectric Properties of PEO-PMMA Blend Based Polymer Nanocomposites. *J. Polym. Res.* **2018**, *25* (5), 116.

(25) Glynos, E.; Petropoulou, P.; Mygiakis, E.; Nega, A. D.; Pan, W.; Papoutsakis, L.; Giannelis, E. P.; Sakellariou, G.; Anastasiadis, S. H. Leveraging Molecular Architecture to Design New, All-Polymer Solid Electrolytes with Simultaneous Enhancement in Modulus and Ionic Conductivity. *Macromolecules* **2018**, *51* (7), 2542−2550.

(26) Pal, P.; Ghosh, A. Influence of TiO_2 Nano-Particles on Charge Carrier Transport and Cell Performance of PMMA-$LiClO_4$ Based Nano-Composite Electrolytes. *Electrochim. Acta* **2018**, *260*, 157−167.

(27) Pan, J.; Zhang, Y.; Wang, J.; Bai, Z.; Cao, R.; Wang, N.; Dou, S.; Huang, F. A Quasi-Double-Layer Solid Electrolyte with Adjustable Interphases Enabling High-Voltage Solid-State Batteries. *Adv. Mater.* **2022**, *34* (10), No. 2107183.

(28) Wang, F.; Li, L.; Yang, X.; You, J.; Xu, Y.; Wang, H.; Ma, Y.; Gao, G. Influence of Additives in a PVDF-Based Solid Polymer

Electrolyte on Conductivity and Li-Ion Battery Performance. *Sustainable Energy Fuels* **2018**, *2* (2), 492−498.
(29) Nourisabet, T.; Aval, H. J.; Shidpour, R.; Naji, L. Fabrication of a PEO-PVDF Blend Based Polymer Composite Electrolyte with Extremely High Ionic Conductivity via the Addition of LLTO Nanowires. *Solid State Ionics* **2022**, *377*, No. 115885.
(30) Tominaga, Y.; Nakano, K.; Morioka, T. Random Copolymers of Ethylene Carbonate and Ethylene Oxide for Li-Ion Conductive Solid Electrolytes. *Electrochim. Acta* **2019**, *312*, 342−348.
(31) Young, W.-S.; Epps, T. H., III Ionic Conductivities of Block Copolymer Electrolytes with Various Conducting Pathways: Sample Preparation and Processing Considerations. *Macromolecules* **2012**, *45* (11), 4689−4697.
(32) Falco, M.; Simari, C.; Ferrara, C.; Nair, J. R.; Meligrana, G.; Bella, F.; Nicotera, I.; Mustarelli, P.; Winter, M.; Gerbaldi, C. Understanding the Effect of UV-Induced Cross-Linking on the Physicochemical Properties of Highly Performing PEO/LiTFSI-Based Polymer Electrolytes. *Langmuir* **2019**, *35* (25), 8210−8219.
(33) Fu, F.; Lu, W.; Zheng, Y.; Kai, C.; Chen, S.; et al. Regulating Lithium Deposition via Bifunctional Regular-Random Cross-Linking Network Solid Polymer Electrolyte for Li Metal Batteries. *J. Power Sources* **2021**, *484*, No. 229186, DOI: 10.1016/j.jpowsour.2020.229186.
(34) Liu, M.; Zhang, S.; Li, G.; Wang, C.; Li, B.; Li, M.; Wang, Y.; Ming, H.; Wen, Y.; Qiu, J.; et al. A Cross-Linked Gel Polymer Electrolyte Employing Cellulose Acetate Matrix and Layered Boron Nitride Filler Prepared via In Situ Thermal Polymerization. *J. Power Sources* **2021**, *484*, No. 229235.
(35) Mardegan, L.; Dreessen, C.; Sessolo, M.; Tordera, D.; Bolink, H. J. Stable Light-Emitting Electrochemical Cells using Hyperbranched Polymer Electrolyte. *Adv. Funct. Mater.* **2021**, *31* (42), No. 2104249.
(36) Zhang, L.; Wang, S.; Li, J.; Liu, X.; Chen, P.; Zhao, T.; Zhang, L. A Nitrogen-Containing All-Solid-State Hyperbranched Polymer Electrolyte for Superior Performance Lithium Batteries. *J. Mater. Chem. A* **2019**, *7* (12), 6801−6808.
(37) Li, Y.-J.; Fan, C.-Y.; Zhang, J.-P.; Wu, X.-L. A Promising PMHS/PEO Blend Polymer Electrolyte for All-Solid-State Lithium Ion Batteries. *Dalton Trans.* **2018**, *47* (42), 14932−14937.
(38) Jinisha, B.; Anilkumar, K.; Manoj, M.; Pradeep, V.; Jayalekshmi, S. Development of a Novel Type of Solid Polymer Electrolyte for Solid State Lithium Battery Applications Based on Lithium Enriched Poly(ethylene oxide)(PEO)/Poly(vinyl pyrrolidone)(PVP) Blend Polymer. *Electrochim. Acta* **2017**, *235*, 210−222, DOI: 10.1016/j.electacta.2017.03.118.
(39) Fu, C.; Ma, Y.; Zuo, P.; Zhao, W.; Tang, W.; Yin, G.; Wang, J.; Gao, Y. In-Situ Thermal Polymerization Boosts Succinonitrile-Based Composite Solid-State Electrolyte for High Performance Li-Metal Battery. *J. Power Sources* **2021**, *496*, No. 229861.
(40) Saeed, A. M. N.; Hezam, A.; Al-Gunaid, M. Q.; TE, S.; Siddaramaiah. Effect of Ethylene Carbonate on Properties of PVP-$CsAlO_2$-$LiClO_4$ Solid Polymer Electrolytes. *Polym.-Plast. Technol. Mater.* **2021**, *60* (2), 132−146, DOI: 10.1080/25740881.2020.1793191.
(41) Lei, Z.; Shen, J.; Wang, J.; Qiu, Q.; Zhang, G.; Chi, S.-S.; Xu, H.; Li, S.; Zhang, W.; Zhao, Y.; et al. Composite Polymer Electrolytes with Uniform Distribution of Ionic Liquid-Grafted ZIF-90 Nanofillers for High-Performance Solid-State Li Batteries. *Chem. Eng. J.* **2021**, *412*, No. 128733.
(42) An, H.; Liu, Q.; An, J.; Liang, S.; Wang, X.; Xu, Z.; Tong, Y.; Huo, H.; Sun, N.; Wang, Y.; et al. Coupling Two-Dimensional Fillers with Polymer Chains in Solid Polymer Electrolyte for Room-Temperature Dendrite-Free Lithium-Metal Batteries. *Energy Storage Mater.* **2021**, *43*, 358−364.
(43) Bae, J.; Li, Y.; Zhao, F.; Zhou, X.; Ding, Y.; Yu, G. Designing 3D Nanostructured Garnet Frameworks for Enhancing Ionic Conductivity and Flexibility in Composite Polymer Electrolytes for Lithium Batteries. *Energy Storage Mater.* **2018**, *15*, 46−52.
(44) Zheng, Y.; Yao, Y.; Ou, J.; Li, M.; Luo, D.; Dou, H.; Li, Z.; Amine, K.; Yu, A.; Chen, Z. A Review of Composite Solid-State Electrolytes for Lithium Batteries: Fundamentals, Key Materials and Advanced Structures. *Chem. Soc. Rev.* **2020**, *49* (23), 8790−8839.
(45) Qian, X.; Gu, N.; Cheng, Z.; Yang, X.; Wang, E.; Dong, S. Impedance Study of $(PEO)_{10}LiClO_4$-Al_2O_3 Composite Polymer Electrolyte with Blocking Electrodes. *Electrochim. Acta* **2001**, *46* (12), 1829−1836.
(46) Wan, J.; Xie, J.; Kong, X.; Liu, Z.; Liu, K.; Shi, F.; Pei, A.; Chen, H.; Chen, W.; Chen, J.; et al. Ultrathin, Flexible, Solid Polymer Composite Electrolyte Enabled with Aligned Nanoporous Host for Lithium Batteries. *Nat. Nanotechnol.* **2019**, *14* (7), 705−711.
(47) Wang, Z.; Shen, L.; Deng, S.; Cui, P.; Yao, X. 10 μm-Thick High-Strength Solid Polymer Electrolytes with Excellent Interface Compatibility for Flexible All-Solid-State Lithium-Metal Batteries. *Adv. Mater.* **2021**, *33* (25), No. 2100353, DOI: 10.1002/adma.202100353.
(48) Huang, X.-W.; Liao, S.-Y.; Liu, Y.-D.; Rao, Q.-S.; Peng, X.-K.; Min, Y.-G. Design, Fabrication and Application of PEO/CMC-Li @PI Hybrid Polymer Electrolyte Membrane in All-Solid-State Lithium Battery. *Electrochim. Acta* **2021**, *389*, No. 138747.
(49) Chattopadhyay, J.; Pathak, T. S.; Santos, D. M. Applications of Polymer Electrolytes in Lithium-Ion Batteries: A Review. *Polymers* **2023**, *15* (19), 3907.
(50) Li, L.; Duan, Y. Engineering Polymer-Based Porous Membrane for Sustainable Lithium-Ion Battery Separators. *Polymers* **2023**, *15* (18), 3690.
(51) Gan, H.; Li, S.; Zhang, Y.; Wang, J.; Xue, Z. Electrospun Composite Polymer Electrolyte Membrane Enabled with Silica-Coated Silver Nanowires. *Eur. J. Inorg. Chem.* **2021**, *2021* (45), 4639−4646.
(52) Sun, J.; Li, Y.; Zhang, Q.; Hou, C.; Shi, Q.; Wang, H. A Highly Ionic Conductive Poly(methyl methacrylate) Composite Electrolyte with Garnet-Typed $Li_{6.75}La_3Zr_{1.75}Nb_{0.25}O_{12}$ Nanowires. *Chem. Eng. J.* **2019**, *375*, No. 121922.
(53) Bai, L.; Wang, P.; Li, C.; Li, N.; Chen, X.; Li, Y.; Xiao, J. Polyaspartate Polyurea-Based Solid Polymer Electrolyte with High Ionic Conductivity for the All-Solid-State Lithium-Ion Battery. *ACS Omega* **2023**, *8*, 20272−20282.
(54) Jang, H. K.; Jung, B. M.; Choi, U. H.; Lee, S. B. Ion Conduction and Viscoelastic Response of Epoxy-Based Solid Polymer Electrolytes Containing Solvating Plastic Crystal Plasticizer. *Macromol. Chem. Phys.* **2018**, *219* (6), No. 1700514.
(55) Lu, Z.; Yang, L.; Guo, Y. Thermal Behavior and Decomposition Kinetics of Six Electrolyte Salts by Thermal Analysis. *J. Power Sources* **2006**, *156* (2), 555−559.

https://doi.org/10.1021/acsomega.4c01669
ACS Omega 2024, 9, 31620−31630